$E1$ moments from a coherent set of measured photoneutron cross sections

S. Goriely,[1] S. Péru,[2,3] G. Colò,[4] X. Roca-Maza,[4] I. Gheorghe,[5] D. Filipescu,[5] and H. Utsunomiya[6]

[1]*Institut d'Astronomie et d'Astrophysique, Université Libre de Bruxelles, Campus de la Plaine, CP-226, 1050 Brussels, Belgium*

[2]*CEA, DAM, DIF, F-91297 Arpajon, France*

[3]*Université Paris-Saclay, CEA, LMCE, 91680 Bruyères-le-Châtel, France*

[4]*Dipartimento di Fisica, Università degli Studi di Milano and INFN, Sezione di Milano, 20133 Milano, Italy*

[5]*National Institute for Physics and Nuclear Engineering, Horia Hulubei (IFIN-HH), 30 Reactorului, 077125 Bucharest-Magurele, Romania*

[6]*Department of Physics, Konan University, 8-9-1 Okamoto, Higashinada, Japan*

(Received 2 November 2020; accepted 24 November 2020; published 9 December 2020)

Recently, the $E1$ photoneutron cross sections were measured consistently using quasimonochromatic laser Compton-scattering γ-ray beams at NewSUBARU (Japan) for a set of ten odd-even nuclei, spherical as well as deformed, covering relatively widely light to heavy species and at energies ranging between the neutron threshold and 40 MeV. This consistent set of experimental photoneutron cross sections allow us to estimate the total $E1$ photoabsorption cross sections, through validated theoretical models, by excluding the quasideuteron component and by including the missing low-energy and charged-particle emission contributions. In turn, the total $E1$ photoabsorption cross sections are used to derive the three main moments of the $E1$ distributions, namely the integrated cross section, the centroid energy, and the polarizability. These so-called model-dependent experimental moments follow a rather smooth trend with atomic mass, as theoretically expected, except for the specific case of ^{209}Bi which presents a surprising 10% increase of both the integrated strength and the polarizability with respect to its even-even spherical neighbor ^{208}Pb. A rather consistent value for the enhancement factor of the $E1$ energy-weighted sum rule could be extracted from the present experimental data. The experimentally derived moments are compared for the ten odd-even systems with calculations based on the mean-field plus quasiparticle random phase approximation (QRPA). Spherical as well as axially deformed predictions based on the Skyrme and Gogny interactions are considered to discuss the results. Special attention is also paid to the approximate treatment of odd systems of nucleons in this context. It is found that in general theoretical predictions can rather well describe the data for the full set of nuclei, except for ^{209}Bi presenting a kink in all the three main $E1$ moments with respect to the well-studied ^{208}Pb case. Such an experimental determination cannot be explained by mean-field plus QRPA calculations. New measurements of photoabsorption cross section on ^{208}Pb and ^{209}Bi in the 14–19 MeV range as well as future theoretical calculations, in particular of odd-even systems, may help to solve such a mystery. The present data are also used to reinvestigate the correlation between the nuclear matter symmetry energy and its slope at saturation density. The analysis based on both Skyrme and Gogny Hartree-Fock-Bogolyubov (HFB) plus QRPA calculations confirm previous results, though quantitatively larger variations of the correlation parameters are found.

DOI: 10.1103/PhysRevC.102.064309

I. INTRODUCTION

Photoneutron cross sections play a key role in the theoretical modeling of nuclear reactions and in our understanding of many properties of both nuclei and nuclear matter. For this reason, they are also important for a wide range of fields such as nuclear structure, nuclear astrophysics, medical isotope production, and fission and fusion reactor technologies. They represent a close measure of the so-called photon strength function (PSF) describing the average response of the nucleus to an electromagnetic probe, including both the photoexcitation and deexcitation of the atomic nucleus by γ-ray absorption or emission [1–3]. Reaction theory relates the PSF to the total photoabsorption cross section that is known to be dominated by the electric dipole ($E1$) radiation, at least in the high γ-ray energy region of 10–20 MeV characterizing the well-known giant dipole resonance (GDR).

Isovector nuclear excitations are also among the most promising observables to extract properties of the so-called symmetry energy and its energy dependence, which play a critical role in nuclear physics and astrophysics [4–8]. Those have been extensively studied from both theoretical and experimental perspectives. Since the symmetry energy cannot be directly measured, many experiments have been designed to extract information about this fundamental quantity from closely related observables. Such experiments include in particular photoabsorption cross section and the resulting electric dipole polarizability of nuclei [9–12].

Photoneutron cross sections (γ, xn) with $x = 1$–4 were recently measured for ten odd-even nuclei at energies ranging

between the neutron threshold and 40 MeV using quasimonochromatic laser Compton-scattering (LCS) γ-ray beams [13–15]. A new method of direct neutron multiplicity sorting was applied [16], which, in combination with several to tens of MeV LCS γ-ray beams, allows complete mapping of the photoneutron reaction cross sections within the GDR energy range. The nuclei include ^{59}Co, ^{89}Y, ^{103}Rh, ^{139}La, ^{159}Tb, ^{165}Ho, ^{169}Tm, ^{181}Ta, ^{197}Au, and ^{209}Bi.

Different mean-field approaches, such as the Hartree-Fock-Bogolyubov (HFB) plus quasiparticle random phase approximation (QRPA), the quasiparticle-phonon model, and some of their improved variants, have been developed and successfully applied to the description of giant multipole resonances in both the nonrelativistic [12,17–35] and relativistic [36–44] mean-field frameworks. When compared with experimental data and considered for practical applications, all mean-field plus QRPA calculations need, however, either some improvement from microscopic many-body theory or some phenomenological corrections. These corrections should include the broadening of the QRPA strength to take into account the damping of collective motion, as well as a shift of the strength to lower energies; both are due to correlations beyond the one-particle–one-hole or two-quasiparticle level, and in particular to the interaction between the single-particle and low-lying collective vibrational degrees of freedom that can also be considered in a fully microscopic framework [27–35,43,44]. In addition, most of the mean-field plus QRPA calculations assume spherical symmetry. Deformed QRPA needs to be adopted or, once again, some phenomenological correction included in order to properly describe the splitting of the giant dipole resonance in deformed nuclei. Essentially all such calculations are performed on even-even nuclei, so that estimates in a system with an odd number of nucleons include approximations. As already mentioned, state-of-the-art calculations including those effects beyond the one-particle–one-hole excitations and phonon coupling are available [27–35,43,44], but they remain restricted to spherical even-even systems and are computationally intractable for large-scale applications. Despite these difficulties, mean-field plus QRPA calculations are well suited to estimate the various moments of the $E1$ strength distributions that, in turn, can provide insight into the effective interaction, and, more particularly, constrain observables like the symmetry energy at the saturation density J, the corresponding slope parameter L, or the neutron skin thickness [8,11,12].

In the present study, the above-mentioned set of ten coherently measured photoneutron cross sections, including nuclei as light as ^{57}Co and as heavy as ^{209}Bi, is considered to extract the main $E1$ moments. In Sec. II, the experimental techniques used to estimate the partial and total photoneutron cross sections are described. In Sec. III we estimate the total $E1$ photoabsorption cross sections and the associated main three moments by excluding the quasideuteron component and including the missing low-energy and charged-particle emission contributions from validated theoretical models. The nonrelativistic mean-field plus QRPA calculations using Skyrme and Gogny interactions considered in the present study are detailed in Sec. IV and their predictions compared with experimental $E1$ moments. In Sec. V, the impact of our study on our understanding of nuclear matter properties, and most of all the symmetry energy, is discussed together with the special case of ^{209}Bi for which the various moments present a clear deviation from the smooth expected trends. The deviations seen in ^{169}Tm as well as the rather consistent experimental description of the energy-weighted sum rule are also discussed in Sec. V. Finally, conclusions are drawn in Sec. VI.

TABLE I. List of targets used for (γ, xn) cross section measurements. The natural abundance of the targets is 100% except for ^{139}La (99.911%) and ^{181}Ta (99.988%). Whenever more than one target thickness is listed, thinner targets were used in (γ, n) cross section measurements below the $2n$ threshold, while thicker targets were used in (γ, xn) cross section measurements above the $2n$ threshold.

Target	Chemical purity (%)	Diameter (mm)	Areal density (g/cm^2)
^{59}Co	99.35	20	5.68
^{89}Y	99.9	10	1.87, 8.99
^{103}Rh	99.9	[a]	8.40
^{139}La	99.9	12.5	3.66, 7.51
^{159}Tb	99.9	20	3.44, 6.74
^{165}Ho	99.9	20	3.52, 3.64, 7.28
^{169}Tm	99.9	20	3.78, 7.40
^{181}Ta	99.99	15	3.34, 6.68
^{197}Au	99.95	20	3.88, 7.75
^{209}Bi	99.9	20	3.95
^{209}Bi	99.9999	12.5	6.97, 9.80

[a]The Rh target consisted of 67 pieces of 1×1 cm^2 foil. The areal density of each foil was 0.1253 ± 0.0010 g/cm^2.

II. EXPERIMENTAL DATA

A Coordinated Research Project (CRP) was launched with the code F41032 by the International Atomic Energy Agency (IAEA) in 2016 to update the preceding photonuclear data library [45]. This IAEA-CRP partially addressed the long-standing discrepancy between the Livermore and Saclay data of total and partial photoneutron cross sections that was left as an unresolved issue in the 2000 library. A series of experiments were also performed to measure the partial photoneutron cross sections for the ten nuclei listed in Table I at the NewSUBARU synchrotron radiation facility within the so-called PHOENIX (photoexcitation and neutron emission cross sections) Collaboration with the Horia Hulubei National Institute for Physics and Nuclear Engineering, Lomonosov Moscow State University, and Shanghai Institute of Applied Physics.

The measured photoneutron cross sections are available in the IAEA Photonuclear Data Library 2019 [3] and at the IAEA Evaluated Photonuclear Data Library website [46]. The key experimental elements in the IAEA-CRP are quasimonochromatic γ-ray beams produced in the inverse Compton scattering of laser photons with relativistic electrons and the methodology of direct neutron-multiplicity sorting with a flat-efficiency detector [16]. Since experimental details are available in the literature [3,13,14,16], we briefly

summarize the key experimental elements and, in addition, describe multiple firings of photoneutron reactions and secondary γ rays generated by the LCS γ-ray beam in passing through a thick target that affect the data reduction.

A. Laser Compton-scattering γ-ray beam

The past measurements carried out in the 20th century at Livermore and Saclay utilized γ-ray beams produced in the positron annihilation in flight. While this γ-ray source had unprecedented features of being quasimonochromatic and energy variable that are suited to excite the GDR and to measure the neutron-decay cross sections, it has the drawback of being accompanied by positron bremsstrahlung produced in a low-Z annihilation target. The positron bremsstrahlung with the end-point energy at the kinetic energy of the positron beam K extended close to the energy of the γ-ray annihilation at $K + 3mc^2/2$. The complication required two separate measurements for background subtraction, one with the positron beam producing annihilation γ rays plus bremsstrahlung and the other with the electron beam producing only bremsstrahlung.

The LCS produced quasimonochromatic and energy-variable γ-ray beams in the energy range from the neutron threshold up to 40 MeV to fully cover the GDR region. It is accompanied by electron synchrotron radiation which, however, concentrates mostly in the keV region far below the quasimonochromatic γ-ray peak [46]. The energy spread of the LCS γ-ray beam was 1% to 3% in the full width at half maximum under good conditions of the electron beam emittance. The energy of the LCS γ-ray beam was precisely calibrated in the order of 10^{-5} [47]. The absolute flux for pulse γ-ray beams was determined with the Poisson-fitting method [48,49]. The capability of the precise energy and flux calibrations of the LCS γ-ray beam is an experimental basis of photoneutron cross section measurements at NewSUBARU.

B. Direct neutron-multiplicity sorting with a flat-efficiency detector

Low energy LCS γ-ray beams were produced with 1064 nm photons from the Nd:YVO_4 INAZUMA laser and used to measure (γ, n) cross sections below the $2n$ threshold by counting the number of neutrons. Above the $2n$ threshold, LCS γ-ray beams were produced with 532 nm photons. The first measurement for ^{209}Bi [13,14], was limited by the minimum operating frequency 16 kHz of the INAZUMA laser; the INAZUMA laser was operated in the second harmonics (532 nm) at 16.66 kHz to produce LCS γ-ray beams with 60 μs pulse intervals. The laser frequency was downscaled by blocking seven out of eight consecutive laser pulses with a Pockels cell and a polarizer to extend the pulse interval to 480 μs. Measurements for nine nuclei from ^{59}Co to ^{197}Au were carried out with a newly introduced Q-switch Talon laser operated at 1 kHz with 1 ms pulse intervals. For the ^{209}Bi measurement, we investigated the effect of the limited time interval of 480 μs on neutron moderation-time curves of the single, double, triple, and quadruple neutron-coincidence events by using GEANT4 simulations [50]. We found that the fraction exceeding the 480 μs time interval amounts to 4% for quadruple events and 1% for single events [13]. Thus, the limited time interval of the ^{209}Bi measurement could not seriously affect the final cross sections.

A flat-efficiency neutron detector (FED) was developed based on the methodology of direct neutron-multiplicity (DNM) sorting as a key experimental element for the IAEA-CRP [16]. In the DNM sorting with FED, one can write a set of equations $\mathbf{N} = \mathbf{F} \cdot \mathbf{R}$ with the number of i-fold neutron events N_i and the number of (γ, xn) reactions R_x ($i, x = 1, 2, 3$, and 4). Here, $N_i = \sum_{x=i}^{4} F_{ix} R_x$ and $F_{ix} = {}_xC_i\, \epsilon^i\, (1-\epsilon)^{x-i}$ with the flat neutron detection efficiency ϵ, which amounts to $36.5 \pm 1.6\%$ (one standard deviation) over the neutron kinetic energy from 10 keV to 5 MeV. One can determine the nondirect experimental observable $\mathbf{R}$ from the direct experimental observable $\mathbf{N}$ by solving the set of equations $\mathbf{R} = \mathbf{F}^{-1} \cdot \mathbf{N}$.

C. Multiple firings and secondary γ rays

The DNM sorting method described above operates under the condition that all neutrons detected during a γ-pulse interval have been associated with a single reaction induced by the given photon pulse. To meet this single-firing condition, the DNM sorting experiments require low reaction rates, which are achieved by appropriate combinations of target thickness, incident γ-ray flux, and reaction cross sections. Still, as the number of photons in an LCS γ-ray pulse follows the Poisson distribution with a typical average value of 10, the incidence of multiple firings can only be minimized, but not completely removed. Experimentally, multiple firings were observed as non-negligible threefold and fourfold neutron events below $3n$ thresholds. Thus, a multiple firing correction is applied to the DNM sorting results, taking into account the target characteristics, incident photon multiplicity, and neutron detection efficiency. The multiple firing correction mostly affects rising and decaying cross sections above the neutron threshold. Multiple firings in a strong decaying channel affect a weak channel on its rising slope of the cross section. The correction amounts up to $\approx$2% for the peak cross sections of all channels measured.

The (γ, xn) experiments made use of thick targets, as listed in Table I, to compensate the relatively low incident photon flux and partial photoneutron cross sections to be measured. Thus, significant fractions of the incident LCS γ-ray beams underwent electromagnetic interactions (pair production, Compton scattering, and photoelectric absorption) in the thick targets. The interactions produce secondary γ rays, which can most efficiently induce photroneutron reactions in the GDR peak energy region generally governed by the (γ, n) channel. Using the GEANT4 package, we simulate the transport of the incident LCS γ-ray beams through the irradiated samples. Photons are tracked along their paths inside the targets to generate a photon energy vs track length histogram which simultaneously accounts for the self attenuation of the incident photon beam, and the production yield and energy spectra of the secondary photons. Details of handling the multiple firings and secondary γ rays in the data reduction can be found in a separate paper [15].

The resulting total photoneutron cross sections $\sigma_\gamma = \sum_{x=1}^{4} \sigma_{(\gamma,xn)}$ are shown in Fig. 1 for the ten odd-even nuclei

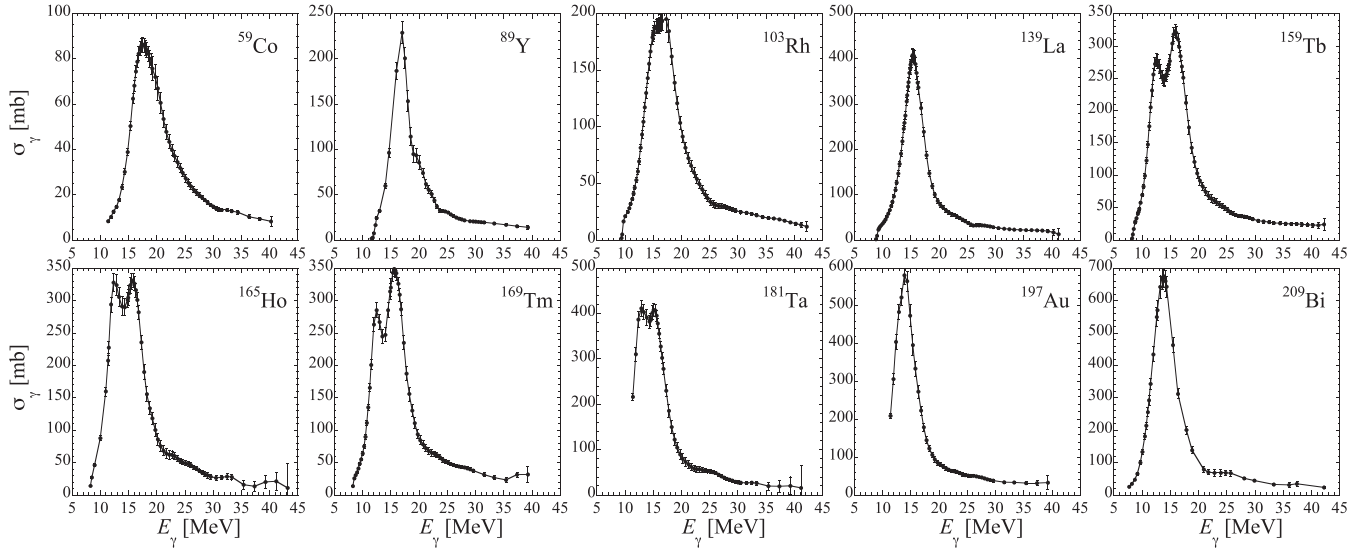

FIG. 1. Measured $E1$ photoneutron cross sections as a function of the photon energy obtained at newSUBARU for the ten odd-even nuclei of interest in the present study.

of interest in the present study, listed in Table I. These cross sections represent a significant set of coherently obtained measurements including nuclei as light as ^{59}Co and as heavy as ^{209}Bi, with different shape properties, namely spherical (^{89}Y, ^{139}La, ^{209}Bi), slightly deformed (^{103}Rh, ^{197}Au), well-deformed (^{159}Tb, ^{165}Ho, ^{169}Tm, ^{181}Ta), or soft vibrational (^{59}Co) nuclei. All of them are odd-even nuclei.

III. EXTRACTION OF THE $E1$ MOMENTS

While the experimental data described in Sec. II provide the full description of the total and partial photoneutron cross sections from the neutron threshold up to 40 MeV, most of the present microscopic mean-field plus QRPA theories cannot provide a detailed account of the PSF, at least without additional corrections. These calculations may, however, provide rather reliable predictions of the main moments of the $E1$ distributions. For this reason, we restrict our theoretical analysis of experimental data to the comparison of the three important $E1$ integrated properties, namely

(i) the integrated cross section $\Sigma_{\rm TRK}$ defined in terms of the Thomas-Reiche-Kuhn (TRK) sum rule $\sigma_{\rm TRK} = 60NZ/A$ mb MeV, i.e.,

$$\Sigma_{\rm TRK} = \frac{1}{\sigma_{\rm TRK}} \times \int_0^\infty \sigma_{abs}(\omega) d\omega, \qquad (1)$$

(ii) the centroid energy

$$E_c = \frac{\int_0^\infty \sigma_{abs}(\omega) d\omega}{\int_0^\infty \sigma_{abs}(\omega)/\omega \, d\omega}, \qquad (2)$$

(iii) and the polarizability

$$\alpha_D = \frac{\hbar c}{2\pi^2 e^2} \int_0^\infty \frac{\sigma_{abs}(\omega)}{\omega^2} d\omega. \qquad (3)$$

From the photoneutron cross sections, it is possible to extract the total $E1$ photoabsorption cross section σ_{abs} over the whole energy region of interest, i.e. up to 40 MeV, provided three model-dependent corrections are applied, namely

(1) The inclusion of a low-energy strength: the photoneutron cross section is measured above the neutron separation energy S_n and is therefore missing at energies below S_n. Also just above S_n, typically about 1–1.5 MeV above the neutron threshold, the photoneutron cross section is sensitive to the neutron channel and may consequently not be representative of the photoabsorption cross section [2]. For this reason, two photon strength function models have been considered to provide the low-energy extrapolations below $S_n + 1.5$ MeV, namely the simple modified Lorentzian (SMLO) model [51,52] and the Gogny-HFB plus QRPA model (based on the D1M interaction and referred to as D1M+QRPA) [2,24]. Both models have been extensively tested and validated on the bulk of experimental PSF data [2]. In the case of ^{209}Bi, as an example, the low-energy correction does not contribute for more than 5% to the polarizability. The differences between SMLO and D1M+QRPA predictions are used to estimate a model uncertainty associated with this low-energy missing strength.

(2) The exclusion of the high-energy quasideuteron contribution: in the high-energy region above typically 20 MeV the experimental dipole strength may be dominated by the nonresonant process in the preequilibrium mode, the so-called quasideuteron component. For a proper comparison with theoretical estimates, this component needs to be subtracted from the experimental cross section. It is estimated through the standard expression [45,53]

$$\sigma_{QD}(E_\gamma) = \mathcal{L}\frac{NZ}{A}\sigma_d(E_\gamma) f(E_\gamma), \qquad (4)$$

TABLE II. Experimental integrated cross sections $\Sigma_{\rm TRK}$, centroid energies E_c, and polarizabilities α_D with their estimated uncertainties (Err) for the ten nuclei considered in the present analysis plus ^{208}Pb on the basis of the data from Ref. [10].

Z	A	$\Sigma_{\rm TRK}$	Err	E_c (MeV)	Err	α_D (fm$^3/e^2$)	Err
27	59	1.15	0.01	19.65	0.23	2.84	0.08
39	89	1.13	0.02	18.35	0.31	4.73	0.14
45	103	1.28	0.01	17.71	0.21	6.90	0.17
57	139	1.31	0.02	16.38	0.20	10.78	0.23
65	159	1.33	0.01	15.83	0.17	13.63	0.27
67	165	1.32	0.03	15.22	0.30	15.11	0.38
69	169	1.25	0.02	15.78	0.20	13.56	0.36
73	181	1.31	0.03	15.03	0.33	16.40	0.65
79	197	1.32	0.02	15.10	0.24	18.04	0.50
82	208	1.29	0.03	14.53	0.29	19.82	0.49
83	209	1.53	0.02	14.93	0.24	22.64	0.51

where σ_d is the experimental deuteron photodisintegration cross section, $f(E_\gamma)$ the Pauli-blocking function, and $\mathcal{L}$ the so-called Levinger parameter. In the case of ^{209}Bi, as an example, the PSF at energies above 20 MeV does not contribute for more than 6% to the polarizability.

(3) The inclusion of the missing charged-particle emission component: the NewSUBARU detection system is not sensitive to the charged-particle emission from the target. For light targets in particular, this charged-particle emission component may contribute significantly to the photoabsorption cross section, especially in the GDR region. To estimate such a contribution, we have made use of the detailed evaluation based on the EMPIRE reaction code [54], which has been carefully adjusted on the present photoneutron cross sections and published in Ref. [3]. For our lightest target ^{59}Co, the charged-particle emission contributes to an increase of the polarizability by 15%, but already no more than 4% for ^{89}Y and even less for the heavier nuclei considered here.

The uncertainties related to each of these model-dependent corrections have been considered and added quadratically to the experimental errors. The final experimental integrated cross sections $\Sigma_{\rm TRK}$, centroid energies E_c, and polarizabilities α_D with their estimated uncertainties are given in Table II. For the sake of comparison, we also include here the relatively well documented case of ^{208}Pb [10]. It will be seen in particular that our determination of the ^{208}Pb polarizability is in good agreement with the results of 19.6 ± 0.6 fm$^3/e^2$ derived in Ref. [12].

IV. THEORETICAL PREDICTIONS

The electric dipole strength $R(\omega; E1)$ is evaluated within the (Q)RPA framework using the dipole operator

$$D = \frac{Z}{A}\sum_{n=1}^{N} r_n Y_{1M}(\hat{r}_n) - \frac{N}{A}\sum_{p=1}^{Z} r_p Y_{1M}(\hat{r}_p), \tag{5}$$

where N, Z, and A are the neutron, proton, and mass numbers, respectively; $r_{n(p)}$ indicates the radial coordinate for neutrons (protons); and $Y_{1M}(\hat{r})$ is the corresponding spherical harmonic. The different $E1$ moments can be estimated with such a definition of the electric dipole strength $R(\omega; E1)$. In particular the polarizability can be expressed as

$$\alpha_D = \frac{8\pi e^2}{9}\int_0^\infty \omega^{-1} R(\omega; E1) d\omega \tag{6}$$

and the centroid energy from the ratio of the first- and zeroth-order moments

$$E_c = \frac{m_1(E1)}{m_0(E1)} = \frac{\int_0^\infty \omega R(\omega; E1) d\omega}{\int_0^\infty R(\omega; E1) d\omega}. \tag{7}$$

Details about the (Q)RPA framework have been extensively published. Here, we restrict ourselves to two frameworks, namely the axially-symmetric-deformed QRPA calculations based on HFB calculations using the finite-range Gogny interaction [22–24,26,55] and the spherical Skyrme-HFBCS plus QRPA calculation [27,56]. Since all the ten nuclei of interest here are odd-even systems, approximations to the mean-field plus QRPA methods are inevitable. The way odd systems have been treated in the Gogny-HFB+QRPA calculations is discussed below.

A. Treatment of odd systems

As mentioned in the Introduction, a consensus in the community about an exact QRPA formulation for odd nuclei is still missing. In a way, this does not impact significantly the main conclusions that the research carried out in the present paper aims to reach. The main moments of the strength distributions (see Sec. III) are not expected to be too sensitive to the addition or removal of a single nucleon; in other words, bulk properties of the strength function are expected to be a smooth function of the nucleon number.

We provide in this subsection some details about the current treatment of the response of odd nuclei in the case of our Gogny-HFB+QRPA calculations, together with some hints for future improvements. We start from the ground-state description. While even-even nuclei are described within HFB, the ground-state of the neighboring odd system is considered as a one-quasiparticle (qp) excitation on top of the HFB vacuum. In the so-called blocking approximation, the occupation probability of the one-qp orbital is imposed. In practice, one needs to select the qp excitation that minimizes the total energy. In the present Gogny-HFB+QRPA calculations, assuming axial symmetry around the z axis and reflection symmetry around the xy plane, the good quantum numbers are the z projection K of the total angular momentum J and the parity π. Thus, the HFB states for odd nuclei with spin-parity J^π are obtained by selecting qp orbitals with $K_1^\pi = J^\pi$ (both quantities are half-integers).

On top of the HFB calculations with blocking, axially symmetric QRPA calculations are performed. A main difference with respect to even-even nuclei is the non-zero value of the ground state spin K_1. In the following, K_2 corresponds to the final state. We remind that the QRPA matrix can be separated in blocks of 2-qp excitations with a given value of

$K \equiv K_2 - K_1$ (we omit parity from here on, for the sake of simplicity). More details can be found in Refs. [55,57]. It has to be stressed here that we exclude from the QRPA valence space the qp orbital which is blocked in the HFB ground state.

Starting from the set of axially symmetric QRPA solutions, states having good angular momentum J and z projection M in the laboratory frame can be obtained through projection techniques. Two different cases should be distinguished. On the one hand, if the nucleus is deformed, projection onto good angular momentum generates a rotational band on top of each QRPA state. On the other hand, if the nucleus is spherical, angular momentum is a good quantum number and only one J value is possible for each QRPA state. Both cases are discussed in more detail below and the results are presented in Sec. IV B.

1. Deformed odd nuclei

An exact projection has been proposed in Ref. [58] and yet never implemented in a systematic way. For well-deformed nuclei, the so-called needle approximation, in which one assumes that the overlap between the wave functions associated with different orientations is negligible, should be reliable. Within such an assumption, the strength function in the laboratory frame is obtained using QRPA reduced matrix elements that read

$$\langle J_2||O_\lambda||J_1\rangle = \sqrt{(2J_1+1)(2J_2+1)}\Bigg[(-)^{J_2-K_2}\begin{pmatrix} J_2 & \lambda & J_1 \\ -K_2 & \mu & K_1\end{pmatrix}\langle\Phi_{K_2}|O_{\lambda\mu}|\Phi_{K_1}\rangle + (-)^{J_2-K_2}\begin{pmatrix} J_2 & \lambda & J_1 \\ -K_2 & \mu' & -K_1\end{pmatrix}(-)^{J_1-K_1}\langle\Phi_{K_2}|O_{\lambda\mu'}|\Phi_{-K_1}\rangle\Bigg]. \quad (8)$$

Here, O is the transition operator for a given multipolarity λ [in the case at hand, $\lambda = 1$ and the operator is the isovector dipole operator of Eq. (5)]. Φ are the intrinsic wave functions that are solutions of HFB plus QRPA. This formula has been proposed in Refs. [39,40,55] for even-even nuclei, where $K_1 = 0$ and the global time-reversal symmetry implies that both terms give the same contribution. In the present case of odd nuclei, sticking to $\lambda = 1$, the second term of the above equation only contributes for $K_1 = 1/2$ and $\mu' = 0, +1$, or $K_1 = -1/2$ and $\mu' = -1, 0$ (following the $3j$ symbols selection rules). For technical reasons, it remains extremely complex to evaluate this extra component, which has consequently not been included in the present Gogny-HFB+QRPA calculation although it may be relevant for ^{103}Rh and ^{169}Tm targets that have a ground-state spin $J = 1/2$.

For a given spin J_1, by imposing a unique $K_1 = J_1$ value, the $E1$ moments are obtained by the sum over all (J_2, K_2) possible contributions. Taking into account all of them with their respective coefficients, the $E1$ moments of odd deformed systems are finally calculated by summing up the intrinsic results for $K = -1, 0, 1$ blocks.

2. Spherical odd nuclei

In the spherical case, the QRPA ground state has already good angular momentum $J_1 = K_1$. This is also true for all QRPA excited states, so that $|J_2(K_2)\rangle \equiv |\Phi_{K_2}\rangle$, where J_2 can be determined elsewhere, since a state with spin J_2 is one of the solutions in all $|K_2| \leqslant J_2$ blocks but not in the $K_2 = J_2 + 1$ block. In this case, the reduced transition probability can be obtained from the intrinsic expression

$$\langle J_2||O_\lambda||J_1\rangle = \frac{(-)^{1-J_2-K_2}}{\sqrt{2J_1+1}}\begin{pmatrix} J_2 & \lambda & J_1 \\ K_2 & \mu & -K_1\end{pmatrix}^{-1}\langle\Phi_2|O_{\lambda\mu}|\Phi_1\rangle. \quad (9)$$

Following the $3j$ symbol selection rules and using occurrences of a J_2 given state in all $|K_2| \leqslant J_2$ blocks of the QRPA calculations, the $E1$ moments are obtained by summing up the intrinsic contributions from all QRPA states of the three $K = -1, 0, 1$ QRPA blocks, i.e., $K_2 = K_1 - 1$, K_1, and $K_1 + 1$, respectively.

B. Axially deformed Gogny-HFB+QRPA calculations

Axially deformed Gogny-HFB plus QRPA predictions obtained with the three D1M, D1S, and D1N interactions [22–24,26,55], including corrections for odd systems (see Sec. IV A), are compared with experimental data in Fig. 2. Clearly, the D1S $E1$ strength is rather shifted to higher energies with respect to D1M and even more to D1N. This confirms the well-established correlation between these $E1$ moments and the nuclear symmetry energy, D1S leading to the softest equation of state of neutron matter, but the highest symmetry energy at saturation (see in particular Figs. 4 and 5 of Ref. [59]). D1N predictions give the best agreement with experimental values of the moments, especially for elements heavier than Rh. D1M overestimates the integrated cross sections and centroid energies, but not significantly more than D1N underestimates them. However, none of the present Gogny-HFB+QRPA calculations can explain the relatively large ^{209}Bi integrated cross section and polarizability, nor the low moments found experimentally for ^{169}Tm relative to the global trend found with the neighboring nuclei.

To check the coherence of the Gogny-HFB plus QRPA predictions for the three moments considered here, we also investigate the impact of an energy shift to the QRPA strength. It is well known that the contribution beyond the one-particle–one-hole excitations and the interaction between the single-particle and low-lying collective phonon degrees of freedom, both neglected by the present QRPA calculations, tend to shift the strength to lower energies [27–29]. In particular, it was found that the Gogny-HFB+QRPA calculations

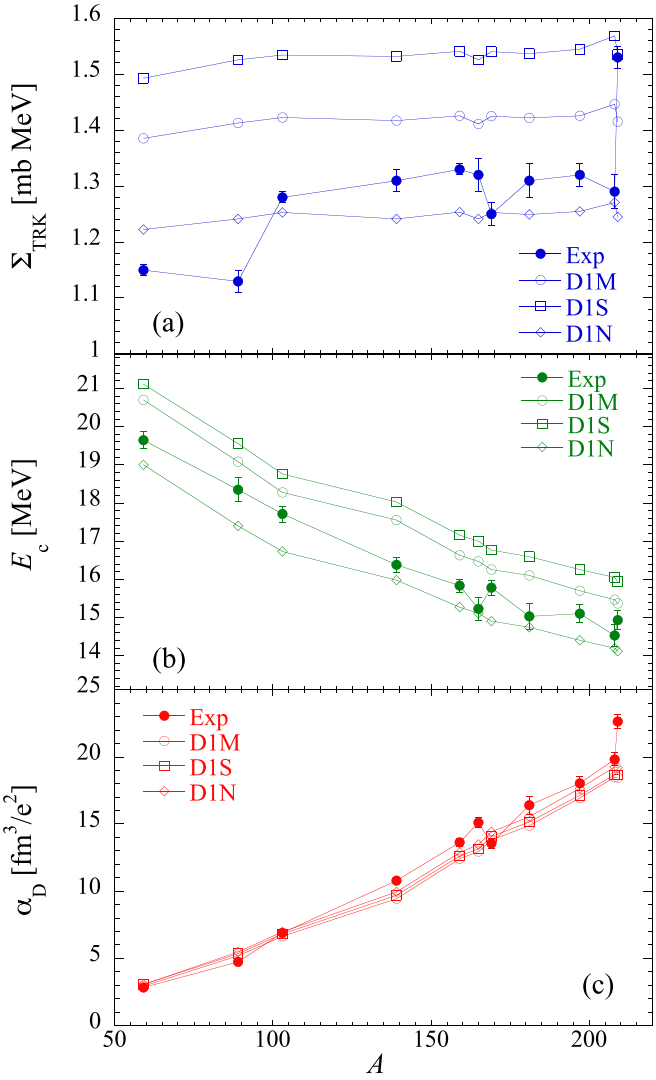

FIG. 2. Comparison between experimental and Gogny-HFB+QRPA predictions based on the D1M, D1S, and D1N interactions (a) for the integrated cross section Σ_{TRK}, (b) the centroid energy E_c, and (c) the polarizability α_D.

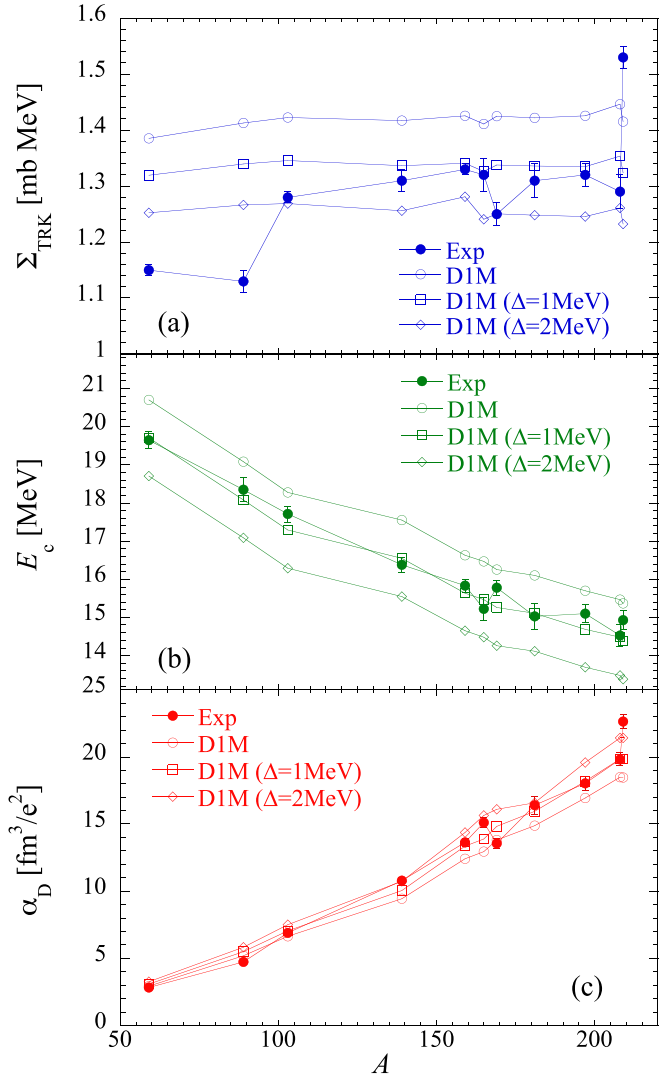

FIG. 3. Comparison between experimental and D1M+QRPA predictions without any energy shift or with a systematic shift Δ of 1 or 2 MeV (a) for the integrated cross section Σ_{TRK}, (b) the centroid energy E_c, and (c) the polarizability α_D.

based on the D1M interaction tend to overestimate the experimental centroid energies by typically 1 to 2 MeV, as shown in Fig. 10 of Ref. [24]. Figure 3 shows the D1M+QRPA predictions together with those obtained by shifting the QRPA strength down in energy by 1 or 2 MeV. While a 2 MeV shift is clearly not favoured by experiments, it can be seen that a systematic shift of 1 MeV down gives rise to moments in rather good agreement with experimental determinations, except for the integrated cross section and polarizability of ^{209}Bi, as well as the integrated cross section of the lightest ^{59}Co and ^{89}Y. At least this comparison shows that, provided some extra correction to go beyond the standard QRPA is included, the three moments can be described rather coherently.

For the three spherical nuclei, ^{89}Y, ^{139}La, and ^{209}Bi, we have tested the impact of the odd number of protons by estimating the three $E1$ moments also on their two respective even-even neighboring isotones. The results are given in Table III for the D1M interaction. It can be seen that with our treatment of the odd systems (see Sec. IV A) the moments of the three odd-Z nuclei do not lie systematically within the range spanned by their neighboring even-Z isotones. We can see that Σ_{TRK} of the odd-Z nucleus is systematically about 2% smaller than the one of its even-Z isotones. Similarly, the centroid energy of the odd-Z is about 1% smaller. Concerning the polarizability, the odd-Z nucleus presents a value rather close to its $Z-1$ isotone, but about 1.5% smaller than the $Z+1$ isotone. The corresponding staggering is seen to increase with increasing mass number with a negligible one for ^{89}Y. This comparison may be used to estimate the moments of the present odd-Z nuclei on the basis of QRPA calculations performed in neighboring even-even nuclei, as discussed in Sec. IV C. Note that the odd-even staggering obtained in Table III is also observed, though sometimes with an unclear pattern, in the experimental GDR properties, including

TABLE III. D1M+QRPA predictions of Σ_{TRK}, centroid energies E_c, and polarizabilities α_D for the three spherical odd-even nuclei of interest in the present study and their even-even neighboring isotones.

Z	A	Σ_{TRK}	E_c (MeV)	α_D (fm^3/e^2)
38	88	1.446	19.298	5.131
39	89	1.413	19.080	5.205
40	90	1.447	19.198	5.338
56	138	1.451	17.647	9.473
57	139	1.417	17.550	9.456
58	140	1.454	17.696	9.636
82	208	1.446	15.470	18.491
83	209	1.415	15.370	18.464
84	210	1.447	15.467	18.764

in particular the energy at the peak cross section (related to the centroid energy) and the integrated photoabsorption cross section Σ_{TRK} [52]. This is true not only along an isotopic chain, but also along an isotone, e.g., along $N = 82$ nuclei for which experimental data are available.

Finally, note that the integrated photoabsorption cross section and the centroid energy can be related to the charge mean square radius and the mean proton distance [60,61] and similarly the polarizability is directly proportional to the mean square radius [12]. Since mean-field models with blocking techniques are known to reproduce rather well charge radii, including the odd-even staggering [62,63], we can expect our blocking approximation in the Gogny-HFB mass model to give a fair, though not complete, representation of the $E1$ moments in odd-even nuclei.

C. Spherical Skyrme-HFBCS plus QRPA calculations

QRPA calculations using the spherical SKYRME_RPA code [56] adapted to include pairing correlations within the Bardeen-Cooper-Schrieffer (BCS) approximation [64] have been performed. We have chosen a delta pairing interaction $V_{pair}(r) = V_0\delta(r)$ where the strength V_0 has been fitted to reproduce the experimental neutron pairing gap in ^{120}Sn with a pairing window considering the first six states above the Fermi level. We have studied six even-even spherical and semimagic nuclei, namely ^{88}Sr and ^{90}Zr, ^{138}Ba and ^{140}Ce, and ^{208}Pb and ^{210}Po, which are neighboring isotones of the measured ^{89}Y, ^{139}La, and ^{209}Bi, respectively. Since the dipole polarizability should be a rather smooth function of the mass number (see Table II), the study of neighboring nuclei may set reasonable upper and lower bounds for the polarizability on the odd-even nucleus. Such an approximation has been tested by the D1M+QRPA calculations performed for the nine above-mentioned nuclei, as detailed in Sec. IV B (see Table III). The TRK enhancement factor as well as the centroid energies for the three odd-even systems ^{89}Y, ^{139}La, and ^{209}Bi are expected to be lower than their even-Z neighboring isotones by typically 1-2%, so that we have extended the lower limit down by 1% on Σ_{TRK} and 2% on E_c. For the polarizability a good approximation is to consider the neighboring $Z-1$ isotone (see Table III), though we have also considered the $Z+1$ isotone as the upper limit. Note that the BCS approximation used in this section is known to reproduce reasonably well HFB results for nuclei close to the valley of β stability [65].

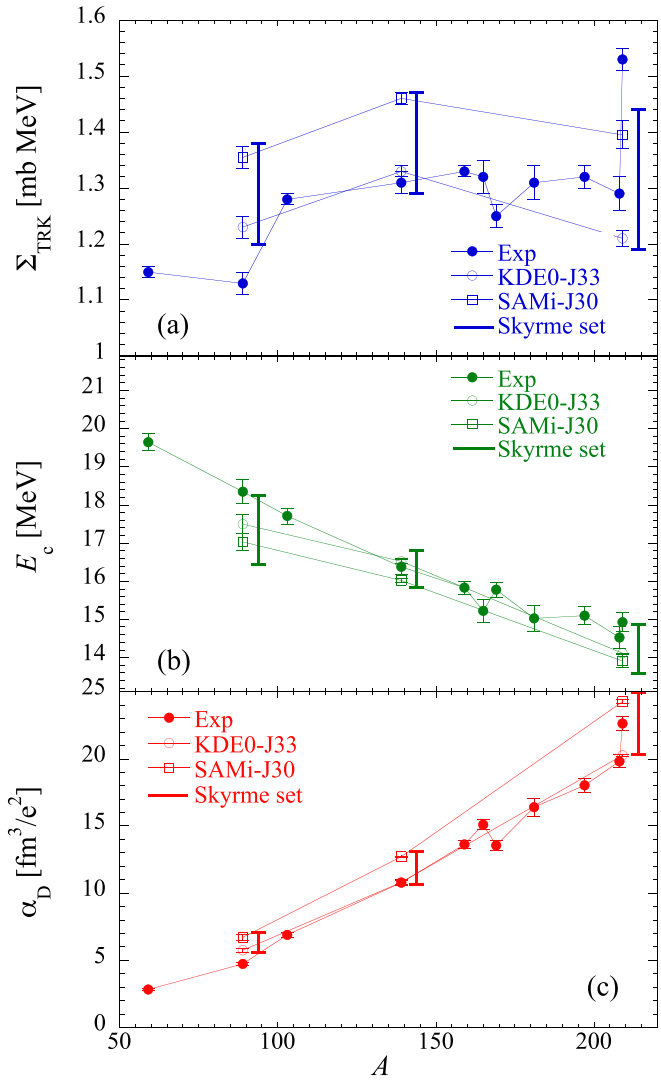

FIG. 4. Comparison between experimental and Skyrme-HF + BCS predictions based on a set of selected functionals (Skyrme set shown as bars slightly shifted to the right) as well as on the KDE0-J30 (empty circles) and SAMi-J30 (empty squares) functionals: (a) for the integrated cross section Σ_{TRK}, (b) the centroid energy E_c, and (c) the polarizability α_D. Only spherical nuclei are compared.

In Fig. 4, we compare graphically the three experimental moments for each of the nuclei reported in Table II with the HFBCS+QRPA calculations as discussed in the previous paragraph. All quantities have been calculated using the same energy range of 0 to 40 MeV as defined by the experimental analysis. Upper and lower theoretical bounds are depicted in Fig. 4 for different Skyrme parametrizations. More specifically, we show the individual results predicted by the KDE0-J33 (empty circles) [66,67] and SAMi-J30 (empty squares) [11,68] functionals as well as an overall prediction (bars slightly shifted right) based on a selected set of

Skyrme functionals of common use in nuclear physics (see also Sec. V A). The latter functionals have been chosen because they predict a large variety of possible values for the symmetry energy at saturation ($27 \lesssim J \lesssim 33$ MeV) and of the slope parameter of the symmetry energy also at saturation ($10 \lesssim L \lesssim 75$ MeV), and the dipole polarizability has been shown to be very sensitive to J and L in medium-heavy and heavy nuclei [12,69]. We explicitly show the limits imposed by the KDE0-J33 functional because it is one of the very few selected functionals able to reproduce the dipole polarizability in different stable and exotic nuclei [12]. As seen in Fig. 4, this functional works reasonably well from a qualitative point of view although it fails in the quantitative description of the experimental data presented here. The predictions of the SAMi-J30 functional are shown because those would be compatible with the large dipole polarizability in ^{209}Bi reported here, which is slightly off the trend followed by the other measured nuclei as a function of the mass number. However, the SAMi-J30 functional is less accurate than KDE0-J33 in the description of the other nuclei as well as on the centroid energy E_c and the energy-weighted sum rule Σ_{TKR}. Overall, bounds are quite spread covering the experimental data reported here, but also showing the relatively large systematic uncertainties of current Skyrme functionals. Finally, note that a coherence check of the Skyrme QRPA predictions of the three $E1$ moments could also be performed, as done through a constant energy shift of the PSF in the D1M+QRPA case in Sec. IV B. Similar results are expected for Skyrme interactions.

V. DISCUSSION

A. Correlation with nuclear matter properties

As already introduced in Sec. I, one of the main motivations to study the isovector dipole response of atomic nuclei is also linked to our understanding of the nuclear symmetry energy and its density dependence. The symmetry energy $S(\rho)$ can be defined through the Taylor expansion of the energy per particle in nuclear matter, E/A, as a function of the density ρ and the isospin asymmetry $\beta = (\rho_n - \rho_p)/\rho$, i.e.,

$$\frac{E}{A}(\rho, \beta) = \frac{E}{A}(\rho, \beta = 0) + S(\rho)\beta^2. \tag{10}$$

If this quadratic approximation in the Taylor expansion is accurate enough, which seems to be the case in most of the realistic calculations, $S(\rho)$ can be viewed as the energy per particle which is needed to change symmetric matter into pure neutron matter at density ρ. The density dependence of this quantity governs the physics of neutron-rich nuclei and neutron stars, as well as many aspects of heavy-ion collisions. For this reason, it is the subject to very intensive investigations and recent review papers [5–7] provide a summary of the main findings. The density dependence around saturation is mainly encoded in the two parameters J and L corresponding, respectively, to the value of the symmetry energy at the saturation density ρ_0 of symmetric matter and to its derivative at the same density.

Isovector nuclear excitations are among the most promising observables to extract properties of the symmetry energy.

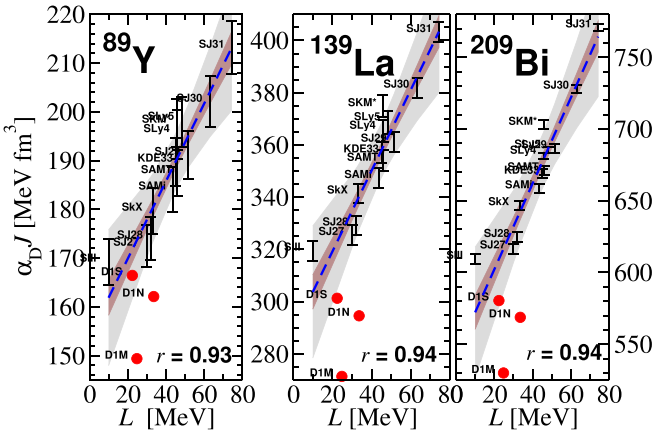

FIG. 5. The dipole polarizability times the symmetry energy at saturation J as a function of the slope parameter at saturation L for (a) ^{89}Y, (b) ^{139}La, and (c) ^{209}Bi are estimated within HFBCS+QRPA for a selected set of Skyrme functionals. The blue dashed line corresponds to a linear fit and the two shaded regions represent the 99.9% and 70% confidence bands.

If nuclei were a piece of nuclear matter with constant density ρ_0, and the isovector GDR were a neutron-proton oscillation mode in which the total density remains constant (so-called Steinwedel-Jensen mode), it follows straightforwardly from Eq. (10) that the isovector GDR energy would be proportional to the second derivative of the energy with respect to β, i.e., to $S(\rho_0)$. As the atomic nucleus is not such a simple classical system, but it has a surface and is affected by quantum shell effects, the relationship between the symmetry energy and the isovector dipole is not so trivial. The topic is reviewed in, e.g., Refs. [8,70].

Among the different features of the dipole response, the advantage of the polarizability defined in Eq. (3) is that its correlation with the symmetry energy is at the same time hinted by the droplet model and obeyed by many nonrelativistic and covariant energy density functionals [11]. One of the purposes of the present work is to see if the conclusions on the values of J and L that have been extracted from a limited set of nuclei, mainly ^{208}Pb and a few other magic or semimagic nuclei, remain true when considering a larger set of nuclei with diverse ground-state properties as studied here (and keeping a coherence within the experimental data).

In Fig. 5, the dipole polarizability times the symmetry energy at saturation, $\alpha_D J$, is displayed as a function of the slope parameter L in the case of the three spherical nuclei ^{89}Y, ^{139}La, and ^{209}Bi. A selected set of Skyrme functionals that cover values of J between 27 and 33 MeV and L between 10 and 75 MeV have been used for the calculations. As in Sec. IV C, we have evaluated the dipole polarizability in the neighboring nuclei, assuming a smooth behavior for this observable, and have provided a range of plausible values for the odd-even systems under investigation. Within this approximate procedure, a clear and strong linear correlation appears for all three nuclei ($r = 0.93$–0.94). The constraints on J and L based on the set of selected Skyrme models are

(in MeV)

$$J = 32.5(1.0) + 0.17(0.02)L \quad \text{for } ^{89}\text{Y},$$
$$J = 26.7(6) + 0.14(0.02)L \quad \text{for } ^{139}\text{La},$$
$$J = 24.0(6) + 0.13(0.01)L \quad \text{for } ^{209}\text{Bi}.$$

As seen in Fig. 5, the Gogny interactions, especially D1N and D1M, do not follow the same trend as Skyrme functionals, the $\alpha_D J$ values for a given L lying significantly lower. If the three Gogny interactions are included in the linear regression shown in Fig. 5, the linear correlation coefficients drop to $r = 0.84$–0.87 and the relation between J and L change to

$$J = 29.5(1.0) + 0.23(3)L \quad \text{for } ^{89}\text{Y},$$
$$J = 22.5(7) + 0.23(4)L \quad \text{for } ^{139}\text{La},$$
$$J = 20.9(6) + 0.19(3)L \quad \text{for } ^{209}\text{Bi}.$$

It is of some interest to compare these findings with those extracted from previous studies based on the experimental dipole polarizability of ^{68}Ni, ^{120}Sn, ^{208}Pb [11,12]. These previously extracted correlations are based on larger set of functionals (48), and lead to rather consistent expressions, namely

$$J = 25.0(2) + 0.19(2)L \quad \text{for } ^{68}\text{Ni},$$
$$J = 25.4(1.1) + 0.17(1)L \quad \text{for } ^{120}\text{Sn},$$
$$J = 24.5(8) + 0.17(1)L \quad \text{for } ^{208}\text{Pb}.$$

If we focus on ^{208}Pb, the correlation between J and L obtained with 48 models does not change at all if we add the three Gogny forces: the Gogny results lie perfectly along the aforementioned correlation (see Fig. 2 of Ref. [11]). If we restrict to the 13 models of the present work, this correlation becomes $J = 26.6(8) + 0.158(16)L$. Consequently, a difference of $\approx$ 10% between the present results and those of [11,12] could be expected because of a different choice of the pool of selected functionals. The reason for the remaining difference is harder to explain. We need further investigations in order to understand to what extent the ground-state deformation, pairing and shell effects, as well as the treatment of odd-even systems, have an impact. In the case of ^{209}Bi, the slope in the correlation between J and L is very small as compared to that of ^{208}Pb when the Gogny results are not considered while it becomes compatible with these results when taken into account.

So, in summary, the correlation between J and L that can be extracted from the analysis of the polarizability on the basis of QRPA calculations remains sensitive to the set of functionals and nuclei considered. The few available Gogny interactions may be compatible with the correlations found with the Skyrme functionals, and the analysis performed for different nuclei gives rise to relatively similar trends of such a correlation with an intercept $J(L = 0) \simeq 21$–32 MeV and a slope $\Delta J/\Delta L \simeq 0.13$–$0.23$. The major uncertainties in these correlation coefficients stem from the diverse predictions with Skyrme or Gogny functionals. In this respect, the uncertainties related to the treatment of odd nuclei, as detailed in Sec. IV A (see in particular Fig. 4), remain rather negligible in comparison with such systematic uncertainties.

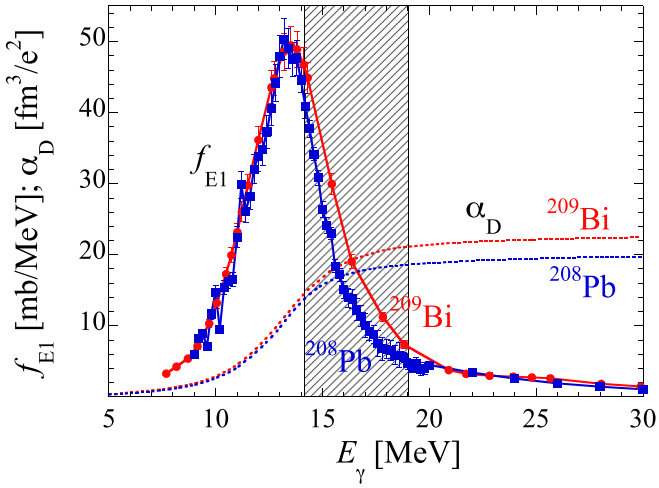

FIG. 6. Comparison between experimental $E1$ PSF (solid lines) of ^{208}Pb (blue squares) and ^{209}Bi (red circles) and the corresponding estimate of the strength contribution to the polarizability α_D (dashed lines).

B. The TRK sum rule

The enhancement factor of the TRK sum rule should also be considered as an important quantity characterizing nuclei and infinite nuclear matter. As it has been often used as a benchmark to fit some of the widely used energy density functionals, setting constraints on its value is certainly an asset. Indeed, the enhancement factor is usually associated with an exchange-force contribution or one of a similar nature, such as nonlocal or velocity-dependent forces. Typical values of the order of 1.20, i.e., 20% of the TRK sum rule, have been extracted from previous experiments [71]. We can see that if we do exclude the lightest $A < 90$ nuclei and the special case of ^{209}Bi (see below), the eight remaining spherical as well as deformed nuclei given in Table II and shown in Figs. 2–4 provide a rather consistent value of about $31 \pm 4\%$. Such a quantity is particularly important to adjust phenomenological models of the electric dipole strength [51,52,72] as well as to improve the adjustment of effective interactions in mean-field approaches, such as those shown in the upper panels of Figs. 2–4. A proper description of the enhancement factor of the TRK sum rule is particularly relevant when such interactions are used directly in QRPA calculations to estimate the PSF.

C. The special case of ^{209}Bi

As given in Table II, the integrated cross section and polarizability of ^{209}Bi are significantly higher than the one of ^{208}Pb, while the centroid energies differ by 0.34 MeV only. The resulting difference in the PSF is illustrated in Fig. 6 together with the integrated polarizability up to a given energy E_γ. Both PSFs present a peak more or less at the same energy and their low-energy tails are rather similar. The major difference clearly comes from the energy range between 14 and 19 MeV, which impacts significantly the estimate of the polarizability, as shown in Fig. 6.

To test further the possibility that the sudden increase of the ^{209}Bi polarizability with respect to ^{208}Pb may be linked to the neutron or proton shell closures, we also estimated the polarizability of ^{58}Ni to compare it with our determination for ^{59}Co. Based on experimental data in Refs. [73,74], we applied the same methodology to estimate the polarizability (as detailed in Sec. III), though without including the charged-particle emission component.

We find for ^{58}Ni $\alpha_D = 2.17 \pm 0.05$ fm$^3/e^2$ with the evaluation of Ref. [74] up to 30 MeV and 2.45 ± 0.09 fm$^3/e^2$ with the measurements of Ref. [73] up to 40 MeV. In the latter case, the polarizability is found to be very similar to the one obtained for ^{59}Co without including the contribution from the charged-particle emission, i.e., 2.46 ± 0.07 fm$^3/e^2$, so that it remains difficult to associate the difference between ^{208}Pb and ^{209}Bi values at least with the proton shell closure.

D. The case of ^{169}Tm

As seen in Table II and Figs. 2–4, ^{169}Tm presents an integrated cross section and polarizability slightly lower (by typically 5%) than found in the global trend with respect to the neighboring nuclei ^{165}Ho or ^{181}Ta. In contrast, its centroid energy is slightly higher. The ^{169}Tm isotope has the specificity to be a deformed nucleus with a $J^\pi = 1/2^+$ ground state. As stressed in Sec. IV A, its polarizability should be calculated using both terms in Eq. (8). According to the sign of the phase for each term of the aforementioned equation, the neglected term could lower the polarizability with respect to neighboring nuclei. It remains, however, difficult to estimate the magnitude of this contribution, so that more studies are needed before drawing any conclusions.

VI. CONCLUSIONS

The photoneutron cross sections have recently been measured using quasimonochromatic laser Compton-scattering γ-ray beams at NewSUBARU (Japan) for ten odd-even nuclei, spherical as well as deformed, covering relatively widely light to heavy species and in a broad energy range covering the neutron threshold up to about 40 MeV. These cross sections have been used here to estimate the three main $E1$ moments, i.e., the integrated cross section, the centroid energy, and the polarizability. Such a determination requires, however, consideration of model-dependent corrections in order to exclude the quasideuteron component and to add the missing low-energy and charged-particle emission contributions. The resulting experimental moments are found to challenge theory in different respects, in particular in the treatment of odd systems. They follow a rather smooth trend with atomic mass, as theoretically expected, except for the specific case of ^{209}Bi which presents a surprising 10% increase of both the integrated strength and the polarizability with respect to its even-even spherical neighbor ^{208}Pb.

We compared the experimentally derived moments for the ten odd-even nuclei with calculations based on the nonrelativistic mean field plus QRPA. Both spherical as well as axially deformed calculations based on both the Gogny and Skyrme interactions have been performed to discuss the results, with special attention paid to the approximate treatment of odd systems of nucleons. It is found that, in general, theoretical predictions can rather well described the data for the full set of nuclei, except for ^{209}Bi presenting this kink in the integrated strength and polarizability with respect to the well-studied ^{208}Pb case. Such an experimental pattern cannot be explained by the present mean-field plus QRPA calculations. New measurements of photoabsorption cross sections on ^{208}Pb and ^{209}Bi in the 14–19 MeV range as well as future theoretical calculation, in particular for odd-even systems, may help to solve such a mystery.

The present data were also used to reinvestigate the correlation between the nuclear matter symmetry energy and its slope at saturation density. The analysis based on both Skyrme and Gogny HFB plus QRPA calculations confirm previous results though quantitatively larger variations of the correlation parameters are found. Finally, a rather consistent value of about 31 ± 4% for the enhancement factor of the TRK sum rule could be extracted from the experimental data of eight out of our ten nuclei.

ACKNOWLEDGMENTS

S.G. acknowledges financial support from FNRS (Belgium). This work was partially supported by the Fonds de la Recherche Scientifique–FNRS and the Fonds Wetenschappelijk Onderzoek–Vlaanderen (FWO) under the EOS Project No. O022818F. G.C. and X.R.-M. acknowledge funding from the European Union Horizon 2020 research and innovation program under Grant Agreement No. 654002. H.U. is grateful for financial support extended to the PHOENIX Collaboration for the IAEA-CRP by the Premier Project of Konan University. D.F. and I.G. acknowledge support from the IAEA CRP on "Updating the Photonuclear Data Library and Generating a Reference Database for Photon Strength Functions" (F41032).

[1] M. Harakeh and A. van der Woude, *Giant Resonances* (Oxford University Press, Oxford, 2001).
[2] S. Goriely, P. Dimitriou, M. Wiedeking, T. Belgya, R. Firestone, J. Kopecky, M. Krticka, V. Plujko, R. Schwengner, S. Siem, H. Utsunomiya, S. Hilaire *et al.*, Eur. Phys. J. A **55**, 172 (2019).
[3] T. Kawano, Y. S. Cho, P. Dimitriou, D. Filipescu, N. Iwamoto, V. Plujko, X. Tao, H. Utsunomiya, V. Varlamov, R. Xu, R. Capote, I. Gheorghe *et al.*, Nucl. Data Sheets **163**, 109 (2020).
[4] J. M. Pearson, N. Chamel, A. F. Fantina, and S. Goriely, Eur. Phys. J. A **50**, 43 (2014).
[5] M. Baldo and G. Burgio, Prog. Part. Nucl. Phys. **91**, 203 (2016).
[6] M. Oertel, M. Hempel, T. Klähn, and S. Typel, Rev. Mod. Phys. **89**, 015007 (2017).
[7] B.-A. Li, B.-J. Cai, L.-W. Chen, and J. Xu, Prog. Part. Nucl. Phys. **99**, 29 (2018).

[8] X. Roca-Maza and N. Paar, Prog. Part. Nucl. Phys. **101**, 96 (2018).
[9] P.-G. Reinhard and W. Nazarewicz, Phys. Rev. C **81**, 051303(R) (2010).
[10] A. Tamii, I. Poltoratska, P. von Neumann-Cosel, Y. Fujita, T. Adachi, C. A. Bertulani, J. Carter, M. Dozono, H. Fujita, K. Fujita, K. Hatanaka, D. Ishikawa *et al.*, Phys. Rev. Lett. **107**, 062502 (2011).
[11] X. Roca-Maza, M. Brenna, B. K. Agrawal, P. F. Bortignon, G. Colò, L.-G. Cao, N. Paar, and D. Vretenar, Phys. Rev. C **87**, 034301 (2013).
[12] X. Roca-Maza, X. Viñas, M. Centelles, B. K. Agrawal, G. Colò, N. Paar, J. Piekarewicz, and D. Vretenar, Phys. Rev. C **92**, 064304 (2015).
[13] I. Gheorghe, H. Utsunomiya, S. Katayama, D. Filipescu, S. Belyshev, K. Stopani, V. Orlin, V. Varlamov, T. Shima, S. Amano, S. Miyamoto, Y.-W. Lui *et al.*, Phys. Rev. C **96**, 044604 (2017).
[14] I. Gheorghe, H. Utsunomiya, S. Katayama, D. Filipescu, S. Belyshev, K. Stopani, V. Orlin, V. Varlamov, T. Shima, S. Amano, S. Miyamoto, Y.-W. Lui *et al.*, Phys. Rev. C **99**, 059901(E) (2019).
[15] I. Gheorghe, D. Filipescu, H. Utsunomiya, S. Belyshev, and K. Stopani (unpublished).
[16] H. Utsunomiya, I. Gheorghe, D. Filipescu, T. Glodariu, S. Belyshev, K. Stopani, V. Varlamov, B. Ishkhanov, S. Katayama, D. Takenaka, T. Ari-izumi, S. Amano *et al.*, Nucl. Instrum. Methods Phys. Res. Sect. A **871**, 135 (2017).
[17] G. Bertsch, Phys. Rev. Lett. **31**, 121 (1973).
[18] K. Liu and G. Borwn, Nucl. Phys. A **265**, 385 (1976).
[19] J. Blaizot and D. Gogny, Nucl. Phys. A **284**, 429 (1977).
[20] E. Khan, N. Van Giai, and M. Grasso, Nucl. Phys. A **731**, 311 (2004).
[21] S. Kamerdzhiev, J. Speth, and G. Tertychny, Phys. Rep. **393**, 1 (2004).
[22] S. Péru and H. Goutte, Phys. Rev. C **77**, 044313 (2008).
[23] S. Péru, G. Gosselin, M. Martini, M. Dupuis, S. Hilaire, and J.-C. Devaux, Phys. Rev. C **83**, 014314 (2011).
[24] M. Martini, S. Péru, S. Hilaire, S. Goriely, and F. Lechaftois, Phys. Rev. C **94**, 014304 (2016).
[25] N. N. Arsenyev, A. P. Severyukhin, V. V. Voronov, and N. Van Giai, Phys. Rev. C **95**, 054312 (2017).
[26] I. Deloncle, S. Péru, and M. Martini, Eur. Phys. J. A **53**, 170 (2017).
[27] G. Colò and P. F. Bortignon, Nucl. Phys. A **696**, 427 (2001).
[28] D. Sarchi, P. Bortignon, and G. Colò, Phys. Lett. B **601**, 27 (2004).
[29] N. Tsoneva and H. Lenske, Phys. Rev. C **77**, 024321 (2008).
[30] P. Papakonstantinou and R. Roth, Phys. Lett. B **671**, 356 (2009).
[31] P. Papakonstantinou, H. Hergert, V. Ponomarev, and R. Roth, Phys. Lett. B **709**, 270 (2012).
[32] P. Papakonstantinou, H. Hergert, and R. Roth, Phys. Rev. C **92**, 034311 (2015).
[33] A. Avdeenkov, S. Goriely, S. Kamerdzhiev, and S. Krewald, Phys. Rev. C **83**, 064316 (2011).
[34] O. Achakovskiy, A. Avdeenkov, S. Goriely, S. Kamerdzhiev, and S. Krewald, Phys. Rev. C **91**, 034620 (2015).
[35] D. Gambacurta, M. Grasso, and O. Vasseur, Phys. Lett. B **777**, 163 (2018).
[36] D. Vretenar, N. Paar, P. Ring, and G. Lalazissis, Nucl. Phys. A **692**, 496 (2001).
[37] P. Ring, Z.-Y. Ma, N. Van Giai, D. Vretenar, A. Wandelt, and L.-G. Cao, Nucl. Phys. A **694**, 249 (2001).
[38] Z.-Y. Ma, A. Wandelt, N. Van Giai, D. Vretenar, P. Ring, and L. Cao, Nucl. Phys. A **703**, 222 (2002).
[39] P. Ring, E. Litvinova, T. Nikšić, N. Paar, D. Peña Arteaga, V. Tselyaev, and D. Vretenar, Nucl. Phys. A **788**, 194 (2007).
[40] D. Peña Arteaga and P. Ring, Phys. Rev. C **77**, 034317 (2008).
[41] I. Daoutidis and S. Goriely, Phys. Rev. C **86**, 034328 (2012).
[42] E. Litvinova and N. Belov, Phys. Rev. C **88**, 031302(R) (2013).
[43] E. Litvinova, P. Ring, and V. Tselyaev, Phys. Rev. C **88**, 044320 (2013).
[44] I. A. Egorova and E. Litvinova, Phys. Rev. C **94**, 034322 (2016).
[45] International Atomic Energy Agency Report No. IAEA-TECDOC-1178, 2000 (unpublished).
[46] IAEA Evaluated Photonuclear Data Library (IAEA/PD-2019), 2020, https://www-nds.iaea.org/photonuclear/
[47] H. Utsunomiya, T. Shima, K. Takahisa *et al.*, IEEE Trans. Nucl. Sci. **61**, 1252 (2014).
[48] T. Kondo, H. Utsunomiya, H. Akimune *et al.*, Nucl. Instrum. Methods Phys. Res. A **659**, 462 (2011).
[49] H. Utsunomiya, T. Watanabe, T. Ari-izumi *et al.*, Nucl. Instrum. Methods Phys. Res. A **896**, 103 (2018).
[50] J. Allison, K. Amako, J. Apostolakis, H. Araujo, P. A. Dubois *et al.*, IEEE Trans. Nucl. Sci. **53**, 270 (2006).
[51] S. Goriely and V. Plujko, Phys. Rev. C **99**, 014303 (2019).
[52] V. Plujko, O. Gorbachenko, R. Capote, and P. Dimitriou, At. Data Nucl. Data Tables **123**, 1 (2018).
[53] M. B. Chadwick, P. Obložinský, P. E. Hodgson, and G. Reffo, Phys. Rev. C **44**, 814 (1991).
[54] M. Herman, R. Capote, M. Sin, A. Trkov, B. Carlson, P. Oblozinsky, C. Mattoon, H. Wienkey, S. Hoblit, Y.-S. Cho, G. Nobre, V. Plujko *et al.*, EMPIRE-3.2 Malta modular system for nuclear reaction calculations and nuclear data evaluation, Brookhaven National Laboratory Techical Report No. BNL-101378-2013, INDC(NDS)-0603, 2013 (unpublished).
[55] S. Péru and M. Martini, Eur. Phys. J. A **50**, 88 (2014).
[56] G. Colò, L. Cao, N. Van Giai, and L. Capelli, Comput. Phys. Commun. **184** (1), 142 (2013).
[57] P. Ring and P. Schuck, *The Nuclear Many-Body Problem* (Springer, Berlin, 2004).
[58] B. Erler and R. Roth, arXiv:1409.0826.
[59] S. Goriely, S. Hilaire, M. Girod, and S. Péru, Eur. Phys. J. A **52**, 202 (2016).
[60] A. Dellafiore and E. Lipparini, Nucl. Phys. A **388**, 639 (1982).
[61] E. Lipparini and S. Stringari, Phys. Rep. **175**, 103 (1989).
[62] E. Verstraelen, A. Teigelhöfer, W. Ryssens, F. Ames, A. Barzakh, M. Bender, R. Ferrer, S. Goriely, P.-H. Heenen, M. Huyse *et al.*, Phys. Rev. C **100**, 044321 (2019).
[63] R. de Groote, J. Billowes, C. Binnersley, M. Bissell *et al.*, Nat. Phys. **16**, 620 (2020).
[64] G. Colò and X. Roca-Maza, user guide and HFBCS-QRPA code, 2020, http://www0.mi.infn.it/~colo/
[65] J. Dobaczewski, W. Nazarewicz, T. R. Werner, J. F. Berger, C. R. Chinn, and J. Dechargé, Phys. Rev. C **53**, 2809 (1996).
[66] B. K. Agrawal, S. Shlomo, and V. K. Au, Phys. Rev. C **72**, 014310 (2005).
[67] B. K. Agrawal *et al.* (private communication).

[68] X. Roca-Maza, G. Colò, and H. Sagawa, Phys. Rev. C **86**, 031306(R) (2012).
[69] X. Roca-Maza, M. Brenna, G. Colò, M. Centelles, X. Viñas, B. K. Agrawal, N. Paar, D. Vretenar, and J. Piekarewicz, Phys. Rev. C **88**, 024316 (2013).
[70] G. Colò, U. Garg, and H. Sagawa, Eur. Phys. J. A **50**, 26 (2014).
[71] B. Berman and S. Fultz, Rev. Mod. Phys. **47**, 713 (1975).
[72] R. Capote, M. Herman, P. Oblozinsky, P. Young, S. Goriely, T. Belgya, A. Ignatyuk, A. Koning, S. Hilaire, V. Plujko, M. Avrigeanu, O. Bersillon *et al.*, Nucl. Data Sheets **110**, 3107 (2009).
[73] B. Ishkhanov, I. Kapitonov, E. Lileeva, E. Shirokov, V. A. Erokhova, M. A. Elkin, and A.V. Izotova, Cross sections of photon absorption by nuclei with nucleon numbers 12–65, Moscow State University, Institute of Nuclear Physics Technical Report No. MSU-INP-2002-27/711, 2002 (unpublished).
[74] V. Varlamov, M. Stepanov, and V. Chesnokov, J. Bull. Russ. Acad. Sci. **67**, 723 (2003).